A Fifth-Order A-WENO Scheme Based on the Low-Dissipation Central-Upwind Fluxes

Shaoshuai Chu, Alexander Kurganov, and Ruixiao Xin

Abstract We introduce a new fifth-order A-WENO scheme based on the low-dissipation central-upwind numerical fluxes recently proposed in [A. Kurganov and R. Xin, preprint]. We apply the developed scheme to the one- and two-dimensional Euler equations of gas dynamics and illustrate its performance on a variety of examples. The obtained numerical results clearly demonstrate that the proposed A-WENO scheme is as robust and at the same time more accurate than the existing A-WENO schemes, which are based on alternative central-upwind fluxes.

1 Introduction

This paper focuses on the development of high-order finite-difference (FD) schemes for hyperbolic systems of conservation laws. We consider one-dimensional (1-D),

$$\boldsymbol{U}_t + \boldsymbol{F}(\boldsymbol{U})_x = \boldsymbol{0}, \tag{1}$$

and two-dimensional (2-D),

$$\boldsymbol{U}_t + \boldsymbol{F}(\boldsymbol{U})_x + \boldsymbol{G}(\boldsymbol{U})_y = \boldsymbol{0}, \tag{2}$$

Shaoshuai Chu
Department of Mathematics, Southern University of Science and Technology, Shenzhen, 518055, China e-mail: chuss2019@mail.sustech.edu.cn

Alexander Kurganov
Department of Mathematics, SUSTech International Center for Mathematics and Guangdong Provincial Key Laboratory of Computational Science and Material Design, Southern University of Science and Technology, Shenzhen, 518055, China e-mail: alexander@sustech.edu.cn

Ruixiao Xin
Department of Mathematics, Southern University of Science and Technology, Shenzhen, 518055, China e-mail: xinrx@mail.sustech.edu.cn

systems. Here, x and y are spatial variables, t is the time, $\boldsymbol{U} \in \mathbb{R}^d$ is a vector of unknowns, and $\boldsymbol{F}$ and $\boldsymbol{G}$ are the x- and y-flux functions.

It is well-known that solutions of (1) and (2) may develop very complicated structures that may include shock, rarefaction, and contact waves even when the initial data are infinitely smooth. As one has to compute nonsmooth weak solutions of (1) and (2), these systems should be rewritten in an equivalent integral form and then it is natural to evolve the integral quantities (cell averages of $\boldsymbol{U}$ over the spatial mesh cells) using finite-volume (FV) methods, which form one of the most popular classes of numerical methods for hyperbolic systems of conservation laws; see, e.g., the monographs [10, 19, 31]. There are two types of FV methods: upwind or central ones; see, e.g., [13]. While upwind schemes typically contain smaller amount of numerical dissipation than the central schemes, central schemes are more robust and often can be applied to a variety of hyperbolic systems in a "black-box" manner. In order to reduce the amount of numerical dissipation present in central schemes, a new class of FV schemes—central-upwind (CU) schemes—was introduced in [16, 17]. These schemes enjoy all of the advantages of the central schemes, while incorporating a certain upwinding information to reduce the numerical dissipation, which was further reduced in [8, 14] and very recently in [3] and [18]. Development of a higher-order extension of the latter CU scheme is the main goal of the current paper.

Many of the FV methods, including the CU schemes, admit a semi-discrete form, which is based on the numerical fluxes that need to be evaluated along the cell interfaces. Typically, the numerical fluxes depend on the left- and right-sided point values of the approximate solution, which are obtained using a global (in space) piecewise polynomial interpolant, reconstructed out of the available cell averages. The reconstruction has to be sufficiently accurate and non-oscillatory. The latter property is ensured using a certain nonlinear limiting mechanism. Second-order FV methods employ second-order piecewise linear reconstructions, which are based on slope limiters; see, e.g., [10, 21, 19, 31] and references therein. Higher-order FV methods require higher-order reconstructions, which are, especially in the multidimensional case, rather complicated and also computationally expensive. For several existing high-order FV methods, we refer the reader to [1, 6, 20, 27, 28] and references therein.

High-order FD schemes offer a simple and less computationally expensive alternative to the FV methods. Weighted essentially non-oscillatory (WENO) FD schemes based on 1-D WENO interpolations constructed in every spatial direction are among the most popular high-order FD schemes. The first WENO FD scheme was proposed in [11]; also see [2, 4, 29, 27, 28] and reference therein. However, these schemes are based on a quite diffusive flux splitting required to stabilize them, and this may affect the quality of the computed solution. A way to overcome the necessity of using any flux splitting was proposed in [12], where alternative WENO (A-WENO) schemes were introduced. A-WENO schemes employ particularly accurate and robust WENO-Z interpolations (see [5, 12, 23, 34]), applied to the characteristic variables using the local characteristic decomposition (LCD) technique (see, e.g., [5, 12, 23, 25, 28, 34]) and achieve very high resolution; see, e.g., [32, 33, 34].

We note that a common strategy often followed while WENO and A-WENO schemes are implemented is based on the fact that high-order WENO reconstructions/interpolations would ensure high accuracy even when the numerical flux is quite dissipative. Therefore, the A-WENO schemes in [5, 23, 34] employed the simplest—yet very robust—central (local Lax-Friedrichs, Rusanov) flux, while in [12] several upwind fluxes have been tested as well. In our recent works [32, 33], we explored a possibility of using less dissipative central and CU fluxes in the context of A-WENO schemes.

In this paper, we develop a new fifth-order A-WENO scheme based on the recently proposed low-dissipation CU (LDCU) numerical fluxes, which have substantially lower amount of numerical dissipation compared with their predecessors. The LDCU numerical fluxes are based on an extremely sharp "built-in" anti-diffusion terms; see the derivation of the semi-discrete LDCU schemes in [18]. We implement the new fifth-order A-WENO scheme for the 1-D and 2-D Euler equations of gas dynamics and demonstrate that the use of the LDCU fluxes leads to an improved resolution without sacrificing the robustness.

2 Fifth-Order A-WENO Schemes

We present the new 1-D and 2-D A-WENO schemes. As the novel feature of the proposed schemes is related to the incorporation of the recently proposed LDCU fluxes into the A-WENO framework, we give a very brief description only.

One-Dimensional Schemes. Assume that the computational domain is covered with uniform cells $[x_{j-\frac{1}{2}}, x_{j+\frac{1}{2}}]$ of size $x_{j+\frac{1}{2}} - x_{j-\frac{1}{2}} \equiv \Delta x$ centered at $x_j = (x_{j-\frac{1}{2}} + x_{j+\frac{1}{2}})/2$ and that the point values $\boldsymbol{U}_j(t)$ are available at a certain time $t \geq 0$. From here on, we suppress the time-dependence of all of the indexed quantities for the sake of brevity.

According to the A-WENO approach introduced in [12], the numerical solution of (1) is evolved in time by solving the following system of ODEs:

$$\frac{\mathrm{d}\boldsymbol{U}_j}{\mathrm{d}t} = -\frac{\boldsymbol{\mathcal{F}}_{j+\frac{1}{2}} - \boldsymbol{\mathcal{F}}_{j-\frac{1}{2}}}{\Delta x},$$

where $\boldsymbol{\mathcal{F}}_{j+\frac{1}{2}}$ are fifth-order accurate numerical fluxes given by

$$\boldsymbol{\mathcal{F}}_{j+\frac{1}{2}} = \boldsymbol{\mathcal{F}}^{\mathrm{FV}}_{j+\frac{1}{2}} - \frac{(\Delta x)^2}{24}(\boldsymbol{F}_{xx})_{j+\frac{1}{2}} + \frac{7(\Delta x)^4}{5760}(\boldsymbol{F}_{xxxx})_{j+\frac{1}{2}}.$$

Here, $\boldsymbol{\mathcal{F}}^{\mathrm{FV}}_{j+\frac{1}{2}} = \boldsymbol{\mathcal{F}}^{\mathrm{FV}}_{j+\frac{1}{2}}\left(\boldsymbol{U}^-_{j+\frac{1}{2}}, \boldsymbol{U}^+_{j+\frac{1}{2}}\right)$ is a FV numerical flux, $\boldsymbol{U}^-_{j+\frac{1}{2}}$ and $\boldsymbol{U}^+_{j+\frac{1}{2}}$ are the left- and right-sided values of $\boldsymbol{U}$ at $x = x_{j+\frac{1}{2}}$ computed using an appropriate WENO-type interpolation. In the numerical results reported in Sect. 3, $\boldsymbol{U}^{\pm}_{j+\frac{1}{2}}$ have been computed using the fifth-order WENO-Z interpolation applied to the local characteristic variables (for details, see, e.g., [5, 12, 23, 34]). Finally, $(\boldsymbol{F}_{xx})_{j+\frac{1}{2}}$ and $(\boldsymbol{F}_{xxxx})_{j+\frac{1}{2}}$ are the

higher-order correction terms computed by the fourth- and second-order accurate finite differences, respectively:

$$\begin{aligned}(\boldsymbol{F}_{xx})_{j+\frac{1}{2}} &= \frac{-5\boldsymbol{F}_{j-2}+39\boldsymbol{F}_{j-1}-34\boldsymbol{F}_{j}-34\boldsymbol{F}_{j+1}+39\boldsymbol{F}_{j+2}-5\boldsymbol{F}_{j+3}}{48(\Delta x)^2},\\ (\boldsymbol{F}_{xxxx})_{j+\frac{1}{2}} &= \frac{\boldsymbol{F}_{j-2}-3\boldsymbol{F}_{j-1}+2\boldsymbol{F}_{j}+2\boldsymbol{F}_{j+1}-3\boldsymbol{F}_{j+2}+\boldsymbol{F}_{j+3}}{2(\Delta x)^4},\end{aligned} \tag{3}$$

where $\boldsymbol{F}_j := \boldsymbol{F}(\boldsymbol{U}_j)$.

We introduce a new A-WENO scheme based on the LDCU numerical fluxes $\boldsymbol{\mathcal{F}}^{\rm FV}_{j+\frac{1}{2}}$, proposed in [18]. In Sect. 3, we compare the performance of the new schemes with the A-WENO scheme based on the CU Rankine-Hugoniot (CURH) flux from [8], which has already been incorporated into the A-WENO framework in [33]. A description of these CU numerical fluxes is omitted for the sake of brevity.

Two-Dimensional Schemes. 2-D fifth-order A-WENO schemes read as

$$\frac{{\rm d}\boldsymbol{U}_{j,k}}{{\rm d}t} = -\frac{\boldsymbol{\mathcal{F}}_{j+\frac{1}{2},k}-\boldsymbol{\mathcal{F}}_{j-\frac{1}{2},k}}{\Delta x} - \frac{\boldsymbol{\mathcal{G}}_{j,k+\frac{1}{2}}-\boldsymbol{\mathcal{G}}_{j,k-\frac{1}{2}}}{\Delta y}. \tag{4}$$

Here, $\boldsymbol{U}_{j,k}$ is a point value of the computed solution at $(x,y)=(x_j,y_k)$, where (x_j,y_k) is a center of the uniform cell $[x_{j-\frac{1}{2}},x_{j+\frac{1}{2}}]\times[y_{k-\frac{1}{2}},y_{k+\frac{1}{2}}]$ with $x_{j+\frac{1}{2}}-x_{j-\frac{1}{2}}\equiv\Delta x$ and $y_{k+\frac{1}{2}}-y_{k-\frac{1}{2}}\equiv\Delta y$ for all j,k. In (4), $\boldsymbol{\mathcal{F}}_{j+\frac{1}{2},k}$ and $\boldsymbol{\mathcal{G}}_{j,k+\frac{1}{2}}$ are fifth-order accurate numerical fluxes given by

$$\begin{aligned}\boldsymbol{\mathcal{F}}_{j+\frac{1}{2},k} &= \boldsymbol{\mathcal{F}}^{\rm FV}_{j+\frac{1}{2},k} - \frac{(\Delta x)^2}{24}(\boldsymbol{F}_{xx})_{j+\frac{1}{2},k} + \frac{7(\Delta x)^4}{5760}(\boldsymbol{F}_{xxxx})_{j+\frac{1}{2},k},\\ \boldsymbol{\mathcal{G}}_{j,k+\frac{1}{2}} &= \boldsymbol{\mathcal{G}}^{\rm FV}_{j,k+\frac{1}{2}} - \frac{(\Delta y)^2}{24}(\boldsymbol{G}_{yy})_{j,k+\frac{1}{2}} + \frac{7(\Delta y)^4}{5760}(\boldsymbol{G}_{yyyy})_{j,k+\frac{1}{2}},\end{aligned} \tag{5}$$

where $\boldsymbol{\mathcal{F}}^{\rm FV}_{j+\frac{1}{2},k}=\boldsymbol{\mathcal{F}}^{\rm FV}_{j+\frac{1}{2},k}\big(\boldsymbol{U}^-_{j+\frac{1}{2},k},\boldsymbol{U}^+_{j+\frac{1}{2},k}\big)$ and $\boldsymbol{\mathcal{G}}^{\rm FV}_{j,k+\frac{1}{2}}=\boldsymbol{\mathcal{G}}^{\rm FV}_{j,k+\frac{1}{2}}\big(\boldsymbol{U}^-_{j,k+\frac{1}{2}},\boldsymbol{U}^+_{j,k+\frac{1}{2}}\big)$ are numerical fluxes with $\boldsymbol{U}^\pm_{j+\frac{1}{2},k}$ and $\boldsymbol{U}^\pm_{j,k+\frac{1}{2}}$ being the one-sided values of $\boldsymbol{U}$ at $(x,y)=(x_{j+\frac{1}{2}}\pm0,y_k)$ and $(x,y)=(x_j,y_{k+\frac{1}{2}}\pm0)$, respectively. In the numerical results reported in Sect. 3, we have computed these point values using the 1-D fifth-order WENO-Z interpolation applied in the x- and y-directions. Finally, the terms $(\boldsymbol{F}_{xx})_{j+\frac{1}{2},k}$, $(\boldsymbol{F}_{xxxx})_{j+\frac{1}{2},k}$, $(\boldsymbol{G}_{yy})_{j,k+\frac{1}{2}}$, and $(\boldsymbol{G}_{yyyy})_{j,k+\frac{1}{2}}$ in (5) are direct "dimension-by-dimension" extensions of the higher-order correction terms (3).

As in the 1-D case, we introduce a new A-WENO scheme by implementing the LDCU x- and y-directional numerical fluxes $\boldsymbol{\mathcal{F}}^{\rm FV}_{j+\frac{1}{2},k}$ and $\boldsymbol{\mathcal{G}}^{\rm FV}_{j,k+\frac{1}{2}}$ in (5).

3 Numerical Examples

We test the new LDCU-based A-WENO schemes and compare their performance with the performance of the A-WENO schemes based on the CURH numerical fluxes (the studied schemes will be referred to as the LDCU and CURH A-WENO schemes). We consider the 1-D and 2-D Euler equations of gas dynamics, which in the 2-D case read as

$$\begin{aligned}
&\rho_t + (\rho u)_x + (\rho v)_y = 0,\\
&(\rho u)_t + (\rho u^2 + p)_x + (\rho uv)_y = 0,\\
&(\rho v)_t + (\rho uv)_x + (\rho v^2 + p)_y = 0,\\
&E_t + [u(E+p)]_x + [v(E+p)]_y = 0,
\end{aligned} \tag{6}$$

where ρ is the density, u and v are the x- and y-velocities, respectively, p is the pressure, and E is the total energy. The system is completed through the equation of state $p = (\gamma - 1)\left[E - \frac{\rho}{2}(u^2 + v^2)\right]$, where γ represents the specific heat ratio. In Examples 1 and 2, we will consider the 1-D version of the system (6), which is obtained by assuming that all of the quantities in (6) are independent of y and $v \equiv 0$.

In examples 1–5, we take $\gamma = 1.4$, while in Example 6, we set $\gamma = 5/3$. In all of the examples, the time evolution is carried out using the three-stage third-order SSP Runge-Kutta method (see, e.g., [9]) with the CFL number 0.45.

Example 1—Shock-Entropy Wave Interaction Problem. In this example, we consider the shock-entropy problem from [29]. The initial conditions,

$$(\rho, u, p)(x, 0) = \begin{cases} (1.51695, 0.523346, 1.805), & x < -4.5,\\ (1 + 0.1\sin(20x), 0, 1), & x > -4.5, \end{cases}$$

correspond to a forward-facing shock wave of Mach 1.1 interacting with high-frequency density perturbations.

We apply the two studied A-WENO schemes to this problem and compute the solutions until the final time $t = 5$ in the computational domain $[-10, 5]$ on a uniform mesh with $\Delta x = 3/80$ subject to the free boundary conditions. The numerical results are shown in Fig. 1 along with the reference solution computed by the CURH A-WENO scheme on a much finer mesh with $\Delta x = 3/1600$. One can observe that the LDCU A-WENO scheme produces slightly more accurate results compared to those obtained by the CURH A-WENO scheme.

Example 2—Stationary Contact Wave and Traveling Shock and Rarefaction. In the last 1-D example taken from [14], the Riemann initial data,

$$(\rho, u, p)(x, 0) = \begin{cases} (1, -19.59745, 1000), & x < 0.8,\\ (1, -19.59745, 0.01), & \text{otherwise}, \end{cases}$$

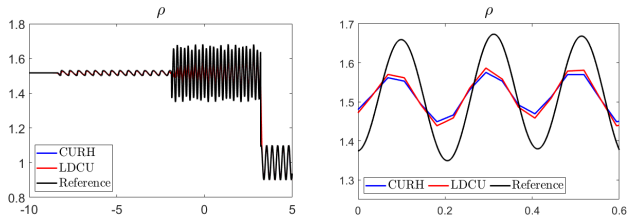

Fig. 1 Example 1: Density (ρ) computed by the CURH and LDCU A-WENO schemes (left) and zoom at $x \in [0, 0.6]$ (right).

are prescribed in the computational domain $[-1, 1]$, in which we impose the free boundary conditions. The exact solution of this initial value problem consists of a stationary contact wave, a traveling shock, and a traveling rarefaction wave.

We compute the CURH and LDCU A-WENO solutions until the final time $t = 0.03$ on a uniform mesh with $\Delta x = 1/100$. The obtained densities together with the reference solution computed using the CURH A-WENO scheme on a much finer uniform mesh with $\Delta x = 1/2000$ are plotted in Fig. 2. As one can see, the LDCU A-WENO scheme achieves a sharper resolution of the contact wave compared to the CURH A-WENO scheme.

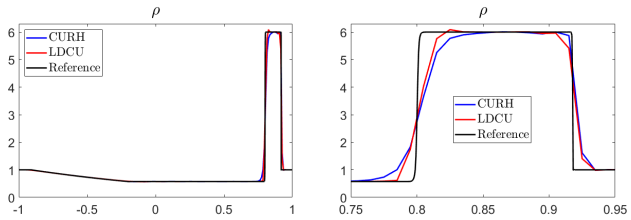

Fig. 2 Example 2: Density (ρ) computed by the CURH and LDCU A-WENO schemes (left) and zoom at $x \in [0.75, 0.95]$ (right).

Example 3—Moving Contact Waves. In the first 2-D test taken from [15], we consider an isolated moving contact wave with the following initial data:

$$(\rho, u, vp)(x, y, 0) = \begin{cases} (1.4, 0, 0.2, 1), & (x, y) \in D \\ (1, 0, 0.2, 1), & \text{otherwise}, \end{cases} \tag{7}$$

prescribed in the computational domain $[-0.2, 0.2] \times [0, 0.8]$, where we impose the free boundary conditions. In (7), the domain D consists of the points (x, y) satisfying the following conditions:

$$\{-0.1 < x < 0.1,\ 0 < y < 0.02\} \cup \{-0.02 < x < 0.02,\ 0.02 < y < 0.1\} \cup$$
$$\{(x + 0.02)^2 + (y - 0.02)^2 < 0.08^2\} \cup \{(x - 0.02)^2 + (y - 0.02)^2 < 0.08^2\}.$$

We compute the numerical solutions until the final time $t = 2$ by the two studied A-WENO schemes on a uniform mesh with $\Delta x = \Delta y = 1/400$ and plot the obtained results in Fig. 3. As one can see, the LDCU A-WENO scheme achieves better resolution of the contact waves in comparison with the CURH A-WENO scheme. Note that the LDCU A-WENO scheme perfectly resolves the non-moving jumps across the lines $x = \pm 0.1$.

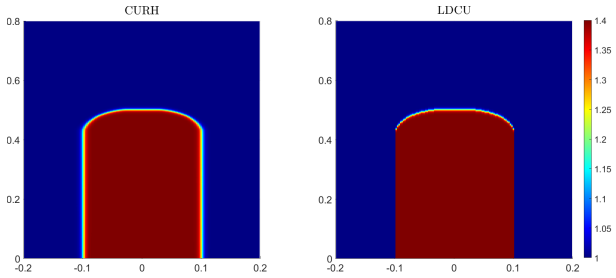

Fig. 3 Example 3: Density (ρ) computed by the CURH (left) and LDCU (right) A-WENO schemes.

Example 4—Implosion Problem. In this example, we consider the implosion problem taken from [8, 14, 22]. The initial conditions,

$$(\rho, u, v, p)(x, y, 0) = \begin{cases} (0.125, 0, 0, 0.14), & |x| + |y| < 0.15, \\ (1, 0, 0, 1), & \text{otherwise}, \end{cases}$$

are prescribed in the computational domain $[0, 0.3] \times [0, 0.3]$ with the solid wall boundary conditions imposed at all of the four sides.

We compute the numerical solutions until the final time $t = 2.5$ on a uniform mesh with $\Delta x = \Delta y = 3/4000$ by the two studied A-WENO schemes. We present the obtained results in Fig. 4, where one can observe that the jets generated by the LDCU A-WENO scheme propagate to a much larger extent compared with the jet produced by the CURH A-WENO scheme. This demonstrates that the LDCU A-WENO scheme contains a substantially smaller amount of numerical dissipation compared with its CURH counterpart.

Example 5—Kelvin-Helmholtz Instability. In this example, we study the Kelvin-Helmholtz instability, which develops in the test problem taken from [7, 8, 24]. We take the following initial data:

$$(\rho(x, y, 0), u(x, y, 0)) = \begin{cases} (1, -0.5 + 0.5e^{(y+0.25)/L}), & y < -0.25, \\ (2, 0.5 - 0.5e^{(-y-0.25)/L}), & -0.25 < y < 0, \\ (2, 0.5 - 0.5e^{(y-0.25)/L}), & 0 < y < 0.25, \\ (1, -0.5 + 0.5e^{(0.25-y)/L}), & y > 0.25, \end{cases}$$

$$v(x, y, 0) = 0.01 \sin(4\pi x), \qquad p(x, y, 0) \equiv 1.5,$$

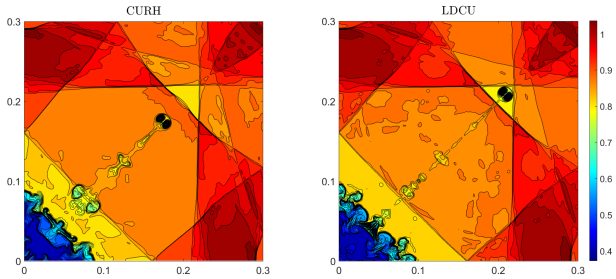

Fig. 4 Example 4: Density (ρ) computed by the CURH (left) and LDCU (right) A-WENO schemes.

where L is a smoothing parameter (we take $L = 0.00625$), which corresponds to a thin shear interface with a perturbed vertical velocity field v in the conducted simulations. Periodic boundary conditions are imposed at all of the four sides of the computational domain $[-0.5, 0.5] \times [-0.5, 0.5]$.

We compute the numerical solutions until the final time $t = 4$ on a uniform mesh with $\Delta x = \Delta y = 1/400$ and plot the obtained results in Fig. 5. As one can see, at time $t = 1$, the vortex sheets formed by the CURH A-WENO scheme are quite smeared by the numerical dissipation, while in the LDCU results these vortex sheets are much more pronounced. At the later time $t = 2.5$, one can observe more complicated vortices and the two-phase turbulence in the "swirls" in the densities computed by the LDCU A-WENO scheme. At the final time $t = 4$, the LDCU solution is quite different from the CURH one and it is actually hard to draw any comparative conclusions about the quality of the obtained results at that time.

Example 6—Rayleigh-Taylor Instability. In the last example taken from [8, 26, 32], we investigate the Rayleigh-Taylor instability, which is a physical phenomenon occurring when a layer of heavier fluid is placed on top of a layer of lighter fluid. The model is governed by the 2-D Euler equations (1), with added gravitational source terms. In the studied setup, the gravitational force acts in the positive y-direction and thus the terms ρ and ρv are added to the third and fourth equations in (6). The resulting system is considered subject to the following initial conditions:

$$(\rho, u, v, p)(x, y, 0) = \begin{cases} (2, 0, -0.025\, c \cos(8\pi x), 2y + 1), & y < 0.5, \\ (1, 0, -0.025\, c \cos(8\pi x), y + 1.5), & \text{otherwise}, \end{cases}$$

where $c := \sqrt{\gamma p/\rho}$ is the speed of sound, the solid wall boundary conditions at $x = 0$ and $x = 0.25$, and the following Dirichlet boundary conditions at the top and bottom boundaries:

$$(\rho, u, v, p)(x, 1, t) = (1, 0, 0, 2.5), \qquad (\rho, u, v, p)(x, 0, t) = (2, 0, 0, 1).$$

We compute the numerical solutions in the computational domain $[0, 0.25] \times [0, 1]$ discretized using a uniform mesh with $\Delta x = \Delta y = 1/800$ until the final time $t = 2.95$. The obtained results are presented in Fig. 6. At earlier time $t = 1.95$, the results

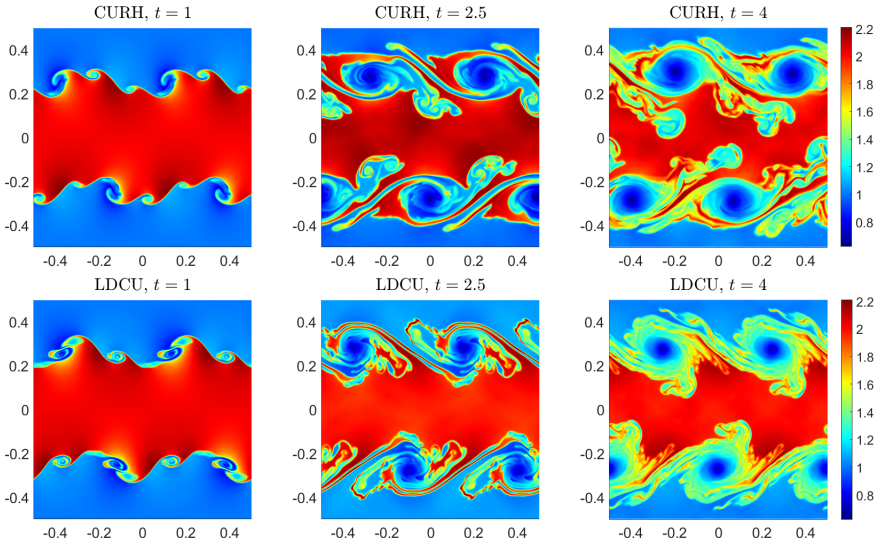

Fig. 5 Example 5: Density (ρ) computed by the CURH (top row) and LDCU (bottom row) A-WENO schemes at three different times.

obtained by the LDCU A-WENO scheme contains more developed mushroom-like structures compared with the results computed by the CURH A-WENO scheme. At the final time $t = 2.95$, one can observe that the LDCU A-WENO scheme captures much more complicated structures than the CURH one. This clearly indicates that the amount of numerical dissipation in the LDCU A-WENO schemes is substantially smaller.

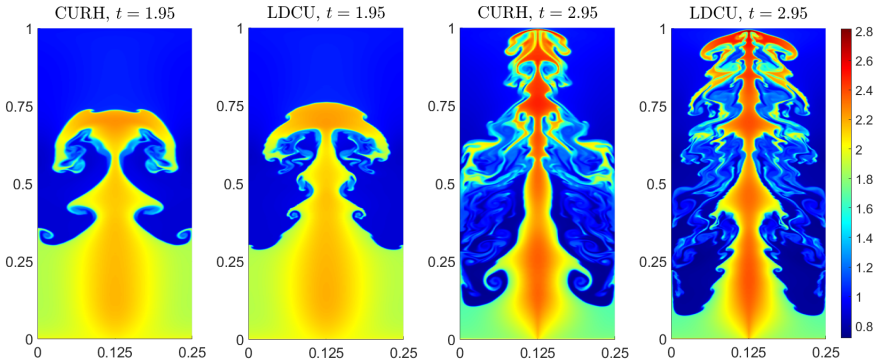

Fig. 6 Example 6: Density (ρ) computed by the CURH and LDCU A-WENO schemes at different times.

Remark 1 It is instructive to compare the CPU times consumed by the two studied schemes. In the 1-D case, the LDCU A-WENO scheme is about 4% more efficient

than the CURH A-WENO scheme. In the 2-D case, the CURH and LDCU A-WENO schemes consume about the same CPU time. This suggests that the proposed LDCU A-WENO scheme outperforms the CURH A-WENO scheme.

Acknowledgements The work of A. Kurganov was supported in part by NSFC grants 12171226 and 12111530004, and by the fund of the Guangdong Provincial Key Laboratory of Computational Science and Material Design (No. 2019B030301001).

References

1. D.S. Balsara, S. Garain, V. Florinski, W. Boscheri, J. Comput. Phys. **404**
2. D.S. Balsara, S. Garain, C.-W. Shu, J. Comput. Phys. **326**
3. A. Chertock, S. Chu, M. Herty, A. Kurganov, M. Lukáčová-Medviďová, J. Comput. Phys. **473**
4. W.S. Don, R. Borges, J. Comput. Phys. **250**
5. W.S. Don, D.-M. Li, Z. Gao, B.-S. Wang, J. Sci. Comput. **82**
6. M. Dumbser, W. Boscheri, M. Semplice, G. Russo, SIAM J. Sci. Comput. **39**
7. U. Fjordholm, S. Mishra, E. Tadmor, Acta Numer. **25**
8. N.K. Garg, A. Kurganov, Y. Liu, J. Comput. Phys. **428**
9. S. Gottlieb, C.-W. Shu, E. Tadmor, SIAM Rev. **43**
10. J.S. Hesthaven, *Numerical Methods for Conservation Laws: From Analysis to Algorithms*. (SIAM, Philadelphia, 2018)
11. G.-S. Jiang, C.-W. Shu, J. Comput. Phys. **126**
12. Y. Jiang, C.-W. Shu, M. Zhang, SIAM J. Sci. Comput. **35**
13. A. Kurganov, in *Handbook of Numerical Methods for Hyperbolic Problems*, ed. by R. Abgrall and C.-W. Shu. Handb. Numer. Anal., vol 17 (Elsevier/North-Holland, Amsterdam, 2016), p. 525
14. A. Kurganov, C.-T. Lin, Commun. Comput. Phys. **2**
15. A. Kurganov, Y. Liu, V. Zeitlin, ESAIM Math. Model. Numer. Anal. **55**
16. A. Kurganov, S. Noelle, G. Petrova, SIAM J. Sci. Comput. **23**
17. A. Kurganov, E. Tadmor, J. Comput. Phys. **160**
18. A. Kurganov, R. Xin, New low-dissipation central-upwind scheme, Submitted. Preprint available at https://sites.google.com/view/alexander-kurganov/publications
19. R.J. LeVeque, *Finite Volume Methods for Hyperbolic Problems*. (Cambridge University Press, Cambridge, UK, 2002)
20. D. Levy, G. Puppo, G. Russo, SIAM J. Sci. Comput. **24**
21. K.A. Lie, S. Noelle, SIAM J. Sci. Comput. **24**
22. R. Liska, B. Wendroff, SIAM J. Sci. Comput. **25**
23. H. Liu, Appl. Math. Comput. **296**
24. J. Panuelos, J. Wadsley, N. Kevlahan, J. Comput. Phys. **414**
25. J. Qiu, C.-W. Shu, J. Comput. Phys. **183**
26. J. Shi, Y.-T. Zhang, C.-W. Shu, J. Comput. Phys. **186**
27. C.-W. Shu, SIAM Rev. **51**
28. C.-W. Shu, Acta Numer. **5**
29. C.-W. Shu, S. Osher, J. Comput. Phys. **77**
30. G.A. Sod, J. Comput. Phys. **27**
31. E.F. Toro, *Riemann Solvers and Numerical Methods for Fluid Dynamics: A Practical Introduction*, 3rd edn. (Springer-Verlag, Berlin, Heidelberg, 2009)
32. B.S. Wang, W.S. Don, N.K. Garg, A. Kurganov, SIAM J. Sci. Comput. **42** (2020)
33. B.-S. Wang, W.S. Don, A. Kurganov, Y. Liu, Commun. Appl. Math. Comput. Published online on November 1, 2021
34. B.-S. Wang, P. Li, Z. Gao, W.S. Don, J. Comput. Phys. **374**